Electron Interactions and Gap Opening in Graphene Superlattices

Justin C. W. Song,[1,2] Andrey V. Shytov,[3] and Leonid S. Levitov[1]

[1]*Department of Physics, Massachusetts Institute of Technology, Cambridge, Massachusetts 02139, USA*
[2]*School of Engineering and Applied Sciences, Harvard University, Cambridge, Massachusetts 02138, USA*
[3]*School of Physics, University of Exeter, Stocker Road, Exeter EX4 4QL, United Kingdom*

(Received 29 December 2012; published 26 December 2013)

We develop a theory of interaction effects in graphene superlattices, where tunable superlattice periodicity can be used as a knob to control the gap at the Dirac point. Applied to graphene on hexa-boron-nitride (G/h-BN), our theory predicts substantial many-body enhancement of this gap. Tunable by the moiré superlattice periodicity, a few orders of magnitude enhancement is reachable under optimal conditions. The Dirac point gap enhancement can be much larger than that of the minigaps opened by Bragg scattering at principal superlattice harmonics. This naturally explains the conundrum of large Dirac point gaps recently observed in G/h-BN heterostructures and their tunability by the G/h-BN twist angle.

DOI: 10.1103/PhysRevLett.111.266801 PACS numbers: 73.22.Pr, 72.80.Vp

Opening up a band gap in graphene promises to unlock a host of tantalizing new physics [1,2]. It will also enable its technological adoption [3]. Recent attempts to open a gap at the Dirac point (DP) can be broadly classed into two principal strategies: (a) spontaneous excitonic gap from electron-electron interactions [4,5] and (b) inducing A-B sublattice asymmetry through an external potential (e.g., substrate) [6–12]. However, unlike bilayer graphene where (a) succeeds, the vanishing density of states in monolayer graphene suppresses interaction effects. Furthermore, it is experimentally challenging to create a commensurate potential on the lattice scale without generating disorder. So far, neither of these approaches alone has succeeded.

Here, we propose a synergistic approach that relies on strength drawn from combining (a) and (b). As we will see, fully in line with the adage 'the whole is greater than the sum of its parts' the interaction-enhanced Bragg scattering by a relatively weak superlattice potential can lead to large gap values. We show that enhancements can be substantial under realistic conditions. Further, the enhancement is tunable by superlattice wavelength, opening the doorway to engineering interaction effects in graphene.

Here we apply these ideas to G/h-BN superlattices [12–15]. Recent measurements found diverging resistance at DP in a G/h-BN system [16–18]. The insulating state at DP is observed despite the extreme cleanness of the system and when long-range disorder due to charge puddles is screened by gates. Curiously, the large gaps (of order 300 K) depended on twist angle [17]. This was unanticipated by noninteracting models [12]. As we show, these observations are explained naturally by our approach.

The dependence on the twist angle arises because this angle controls the periodicity of G/h-BN moiré patterns (Fig. 1 inset). The wavelengths in moiré superlattices can be as long as 100 atomic distances, depending on both the lattice mismatch and twist angle between graphene and h-BN, $\lambda_0(\theta) \approx \lambda_0\delta/(\theta^2 + \delta^2)^{1/2}$ [6,12]. In turn, the wavelength λ controls the DP gap Δ_0 enhancement via renormalization group (RG) flow (Fig. 1). As a result, Δ_0 can be tuned by θ. Our RG approach predicts a power-law scaling

$$\Delta_0(\theta) \propto [\lambda_0(\theta)/a]^{\gamma}, \tag{1}$$

giving a strong dependence on the twist angle θ. Here $a = 1.42$ Å is the carbon spacing and the value γ is estimated below [see Eq. (15)]. The twist angle-dependent Δ_0 is consistent with recent experimental observations [17]. Our estimates, based on a one-loop RG, show that DP gap values as large as $\Delta_0 \approx 5$–40meV can be realized. The large enhancement predicted by RG originates from the fact that the DP gap arises at third order in a weak superlattice potential. While this suppresses the bare gap value, it also triples the scaling exponent β describing the interaction-induced enhancement [see Eqs. (10) and (11)].

The RG approach complements, in an important way, existing *ab initio* calculations for commensurate and lattice-matched graphene heterostructures. Recently, gaps at DP arising from the sublattice asymmetry of SiC [7–9] and h-BN [10] have been predicted; substrate-induced gaps were observed in epitaxial graphene on SiC [11]. Interaction-enhanced gaps were also analyzed in a commensurate structure [19]. However, experimentally realistic graphene heterostructures are incommensurate and lattice mismatched with relevant superlattice length scales that exceed the atomic scale by almost 2 orders of magnitude. Such large registrations are beyond the capability of *ab initio* techniques, which are typically limited to cell sizes of tens of atoms. On the other hand, the RG approach is ideally suited for describing long wavelength behavior. In this work, we set out to understand the interplay of interactions and incommensurability. While we focus on G/h-BN systems, our approach applies equally to other closely matched substrates such as SiC.

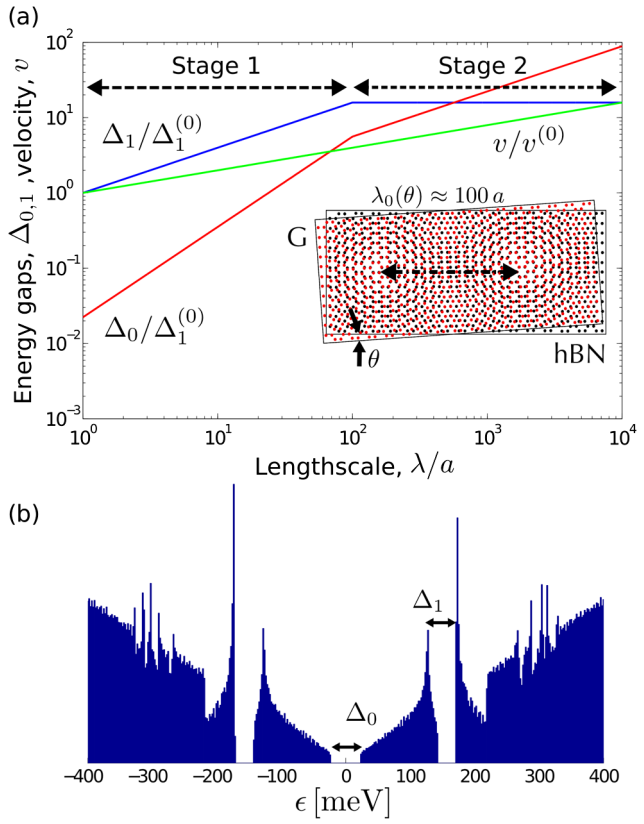

FIG. 1 (color online). (a) Interaction-induced enhancement of couplings to an incommensurate (moiré) superlattice potential. The superlattice spatial wavelength λ, tunable by the twist angle between G and h-BN (inset), controls the interaction effects via RG flow. Renormalization for the DP gap Δ_0 and the gap Δ_1 opened by Bragg scattering at the principal superlattice harmonics is shown by red and blue lines, respectively. Renormalization proceeds in two stages. Both gaps are enhanced from the noninteracting values $\Delta_0^{(0)}$ and $\Delta_1^{(0)}$; however, the gap Δ_0 undergoes a much larger enhancement and, despite a small initial value, eventually overtakes Δ_1. Both Δ_0 and Δ_1 grow faster than the carrier velocity v (green line). (b) Density of states obtained using renormalized gaps and velocity. Parameters used: superlattice period $\lambda_0 = 14$ nm, scaling exponents $\beta = 0.6$ and $\beta_v = 0.3$, and initial values $\Delta_0^{(0)} \approx 0.02\Delta_1^{(0)}$ (see the text).

The origin of a strong effect of interactions on the band structure can be understood as follows. Interacting Dirac particles respond very differently to a scalar external potential which is sublattice blind than to a pseudospin-dependent ("colored") potential reflecting the A-B sublattice modulation. In the first case, interactions generate a polarization that screens the potential. In the second case, interactions generate sublattice correlations that amplify the potential. The interaction-enhanced colored potential leads to pseudospin-dependent Bragg scattering which generates a gap at DP Δ_0. Further, because the Dirac mass term is a relevant perturbation in the RG sense, this gap undergoes a giant interaction-induced enhancement. Interestingly, the resulting Δ_0 value can exceed the side gaps opened by Bragg scattering at principal superlattice harmonics; see Fig. 1.

Because of long-period spatial oscillations in the moiré superlattice, the RG flow proceeds in two separate stages: stage 1 describing renormalization at length scales up to the moiré wavelength $\lambda < \lambda_0$ and stage 2 describing length scales $\lambda > \lambda_0$. The length scale at which the RG terminates is controlled by the screening length which is set by the distance to the gates when those are metallic, as in Ref. [20], or by the screening length in the gate if the latter is realized by a proximal graphene layer, as in Ref. [21]. Stage 1 acts as a "booster," generating an enhancement of energy gaps which is much greater than that of carrier velocity. In stage 2, the growth of the side gap Δ_1 stalls whereas the gap Δ_0 continues to grow. As illustrated in Fig. 1, the gap Δ_0 can eventually overtake Δ_1 even if the latter starts with a larger microscopic bare value. This unusual hierarchy of energy scales $\Delta_0 > \Delta_1$ can serve as a telltale sign of interaction-assisted gap opening.

Turning to the analysis, since the moiré superlattice period is much larger than the lattice constant $\lambda_0 \gg a$, states in valleys K and K' are effectively decoupled. Hence, we can describe each valley by a continuum Hamiltonian with a pseudospin dependence reflecting A-B sublattice modulation and an oscillatory position dependence reflecting the superlattice periodicity:

$$H_0 = \begin{pmatrix} u_{11} f(\mathbf{x}) & v p_- + u_{12} f(\mathbf{x}) \\ v p_+ + u_{21} f(\mathbf{x}) & u_{22} f(\mathbf{x}) \end{pmatrix}, \quad (2)$$

$$f(\mathbf{x}) = 2 \sum_{s=1,2,3} \cos(\mathbf{b}_s \mathbf{x} + \phi_s), \quad (3)$$

$p_\pm = p_x \pm i p_y$. Here, $\mathbf{b}_s$ $(s = 1, 2, 3)$ are three Bravais vectors of the triangular superlattice oriented at 60° angles relative to each other. Introducing pseudospin Pauli matrices $\sigma_{1,2,3}$ and adding long-range interactions, we write

$$\mathcal{H} = \int d^2x \sum_{i=1}^{N} \psi_i^\dagger(\mathbf{x})[v\boldsymbol{\sigma} \cdot \mathbf{p} + m_3(\mathbf{x})\sigma_3 + m_0(\mathbf{x})]\psi_i(\mathbf{x}) + \frac{1}{2} \int d^2x \int d^2x' \frac{e^2}{\kappa|\mathbf{x} - \mathbf{x}'|} n(\mathbf{x}) n(\mathbf{x}'), \quad (4)$$

where $m_3 = \frac{1}{2}(u_{11} - u_{22}) f(\mathbf{x})$ and $m_0 = \frac{1}{2}(u_{11} + u_{22}) f(\mathbf{x})$. Here, $N = 4$ is the number of spin or valley flavors, and $n(\mathbf{x}) = \sum_{i=1,\ldots,N} \psi_i^\dagger(\mathbf{x})\psi_i(\mathbf{x})$ is particle density. The off-diagonal terms u_{12} and u_{21}, which describe a gauge-field coupling generated by strain, can be incorporated in the $v\boldsymbol{\sigma}\mathbf{p}$ term. However, *ab initio* studies [22] indicate that it is a small contribution compared to u_{11} and u_{22}.

The amplitude of sublattice modulation can be inferred from *ab initio* calculations [10] predicting $6(u_{11} - u_{22}) \approx 53$ meV for the equal-period case, $\mathbf{b} = 0$. This gives amplitudes m_3 of individual Bragg harmonics which are more than 20 times smaller than the kinetic energy at the

Bragg vector $\epsilon_0 = \frac{1}{2}\hbar v|\mathbf{b}| \approx 150$ meV estimated for the largest superlattice period $\lambda_0 = 14$ nm [23]. Hence, we can employ perturbation theory in the small ratio m_3/ϵ_0.

The RG analysis of this Hamiltonian predicts that the m_3 harmonics grow under RG, whereas the m_0 harmonics do not grow (see below). Therefore, even if the microscopic values $m_3^{(0)}$ and $m_0^{(0)}$ are comparable, the band gaps will be dominated by the m_3 harmonics. We can therefore estimate the band gap opening at the edge of the superlattice Brillouin zone as $\Delta_1 = 2m_3$.

Importantly, the interaction with the superlattice leads to gap opening at DP. While a single m_3 harmonic is sign changing and cannot give rise to a gap by itself, $\langle e^{i\mathbf{bx}}\rangle = 0$, a combination of three different harmonics can open up a gap at DP. Choosing triplets of harmonics with the sum of their wave vectors adding up to zero $\mathbf{b}_i + \mathbf{b}_j + \mathbf{b}_k = 0$, third-order perturbation theory in m_3 yields a constant sublattice-asymmetric term [24]

$$H_0' = \sum_{\pm\mathbf{b}_i,\pm\mathbf{b}_k} m_3\sigma_3 \frac{1}{v\boldsymbol{\sigma}\cdot\mathbf{b}_i} m_3\sigma_3 \frac{1}{v\boldsymbol{\sigma}\cdot\mathbf{b}_k} m_3\sigma_3 = -\frac{1}{2}\Delta_0\sigma_3, \tag{5}$$

where $\Delta_0 = 12m_3^3/(v|\mathbf{b}|)^2$ [the corresponding self-energy is shown in Fig. 2(a)]. Contributions similar to H_0' can also arise when two out of three $m_3\sigma_3$ terms are replaced by m_0 harmonics. However, since these harmonics do not grow under the RG (see below), these contributions are small. Since $m_3 \ll \epsilon_0$, the predicted numerical value is small $\Delta_0 \ll \Delta_1$ (a similar observation was made in Ref. [6]). However, as we find shortly, the gap Δ_0 undergoes a giant boost due to interaction effects, growing faster than Δ_1. As a result, the physical values Δ_0 and Δ_1 become comparable.

We describe the effect of interactions on the terms m_0 and m_3 in Eq. (4) using the RG approach developed in Refs. [25–27]. There are two distinct flavors of RG, a weak-coupling approach and a large-N approach [5]. The weak-coupling RG, which uses $e^2/\hbar v \ll 1$ as an expansion parameter, does not account for screening of the Coulomb interaction and features logarithmic enhancements. The large-N RG, in contrast, describes strong coupling, fully accounts for screening, and produces power-law enhancements (see below). The two approaches differ quantitatively, yet they lead to qualitatively similar results. Here, we present detailed results for the more realistic large-N approach.

We first treat the m_0 and m_3 terms in Eq. (4) as spatially uniform, ignoring their x dependence. The approach is valid over the range of length scales $a < \lambda \lesssim \lambda_0$. Larger length scales $\lambda \gtrsim \lambda_0$ will be analyzed below. Renormalization is found by dressing the m_0 and m_3 vertices in Feynman diagrams with vertex corrections and analyzing the corresponding log-divergent contributions. The vertex correction for the m_0 term is canceled by a corresponding contribution to the Green's function residue, owing to the Ward identity that follows from gauge invariance. This can be seen more explicitly by analyzing the self-energy

$$\Sigma(\epsilon,\mathbf{p}) = -\int \frac{d\epsilon' d^2p'}{(2\pi)^3} V(\epsilon',\mathbf{p}')G(\epsilon-\epsilon',\mathbf{p}-\mathbf{p}') \tag{6}$$

with $G(\epsilon,\mathbf{p}) = 1/(i\epsilon - v\boldsymbol{\sigma}\cdot\mathbf{p} - m_3\sigma_3 - m_0)$, and V representing the dynamically screened interaction

$$V(\epsilon,\mathbf{p}) = \frac{V_0(\mathbf{p})}{1 - NV_0(\mathbf{p})\Pi(\epsilon,\mathbf{p})}, \qquad V_0(\mathbf{p}) = \frac{2\pi e^2}{\kappa|\mathbf{p}|}. \tag{7}$$

Renormalization of the m_0 coupling, at linear order in m_0, is described by the quantity $\partial_{i\epsilon}\Sigma + \partial_{m_0}\Sigma$ which vanishes due to the form of $G(\epsilon,\mathbf{p})$.

We note that the cancellation of log-divergent contributions due to the Ward identity does not apply to reducible diagrams. The latter generates a vertex correction giving an effective dielectric constant $\tilde{\kappa} = [1 - NV_0(\mathbf{p})\Pi(\epsilon,\mathbf{p})]\kappa$, which describes intrinsic screening of the m_0 vertex by interband and intraband polarization.

Since the m_3 vertex is distinct from the m_0 vertex, we expect that log-divergent contributions do not cancel. As a result, electrons become "colored"; i.e., their coupling to the moiré superlattice potential is dominated by pseudospin-dependent interactions. The renormalization of m_3 was analyzed in Ref. [19], giving a scaling exponent $\beta = 16/\pi^2 N$ which is 2 times larger than the value $\beta_v = 8/\pi^2 N$ found for velocity renormalization in Ref. [27]. This leads to RG flow equations for the m_3 coupling and velocity:

$$\frac{dm_3}{d\xi} = \beta m_3, \qquad \frac{dv}{d\xi} = \beta_v v, \qquad \frac{2\pi}{\lambda_0} < |\mathbf{p}| < p_0, \tag{8}$$

where $\xi = \ln(p_0/|\mathbf{p}|)$ is the RG time parameter, with $p_0 \sim 2\pi/a$ the UV cutoff. Interestingly, the relation $\beta = 2\beta_v$ also holds in the weak-coupling approach. The RG flow [Eq. (8)] predicts a power-law enhancement to the m_3 harmonic and velocity for $a < \lambda < \lambda_0$:

$$m_3 = (\lambda/a)^{\beta} m_3^{(0)}, \qquad v = (\lambda/a)^{\beta_v} v^{(0)}. \tag{9}$$

Similarly, renormalization of $\Delta_0 \propto m_3^3/v^2$ is obtained by adding the contributions shown in Figs. 2(b) and 2(c):

$$\frac{\partial\Sigma}{i\partial\epsilon} + \frac{3\delta\Sigma}{\delta(\sigma_3 m_3)} - \frac{2\delta\Sigma}{\delta(v\boldsymbol{\sigma}\mathbf{p})} = \int \frac{d\epsilon' d^2p'}{(2\pi)^3}\Big[\frac{V(\epsilon',\mathbf{p}')}{(i\epsilon' - v\boldsymbol{\sigma}\mathbf{p}')^2} - \frac{3V(\epsilon',\mathbf{p}')}{(i\epsilon' - v\boldsymbol{\sigma}\mathbf{p}')(i\epsilon' + v\boldsymbol{\sigma}\mathbf{p}')} - \frac{2V(\epsilon',\mathbf{p}')\epsilon'^2}{(i\epsilon' - v\boldsymbol{\sigma}\mathbf{p}')^2(i\epsilon' + v\boldsymbol{\sigma}\mathbf{p}')^2}\Big]$$
$$\approx (3\beta - 2\beta_v)\ln\frac{p_0}{|\mathbf{p}|}, \tag{10}$$

where we integrate over $|\mathbf{p}| \le p' \le p_0$. Taking N to be large, we find the value $32/\pi^2 N$ which is 2 times larger than the exponent β found in Ref. [19] and 4 times larger

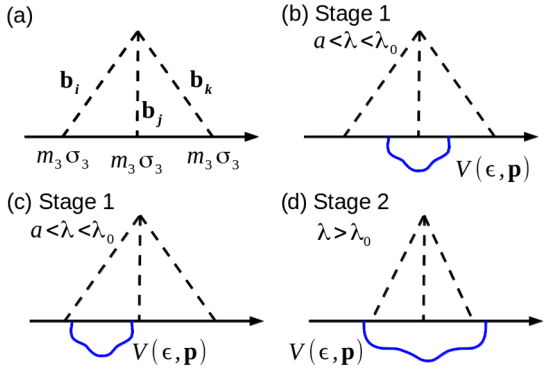

FIG. 2 (color online). (a) Self-energy describing a gap opening at the Dirac point due to the bare sublattice-asymmetric superlattice potential [see Eq. (5)]. (b)–(d) Log-divergent diagrams contributing to gap renormalization at one loop. Here, solid black lines represent the electron Green's function $G(\epsilon, \mathbf{p})$, dashed lines represent coupling to the sublattice-asymmetric potential [the term $m_3\sigma_3$ in Eq. (4)], and the wavy lines represent the Coulomb interaction. (b) Vertex renormalization and (c) velocity renormalization arise from integration over $|\mathbf{b}| \lesssim |\mathbf{p}| \lesssim p_0$ (stage 1), giving Eq. (11). The contribution (d) arises from $|\mathbf{p}| < |\mathbf{b}|$ (stage 2), giving Eq. (12).

than the exponent β_v. As a result, Δ_0 grows under the RG far faster than Δ_1:

$$\Delta_0 = \frac{12m_3^3}{v^2|\mathbf{b}|^2} = (\lambda/a)^{3\beta-2\beta_v}\Delta_0^{(0)}. \tag{11}$$

A tenfold increase in Δ_1 translates into a 100-fold increase in Δ_0; see Fig. 1. Thus, despite a handicap due to a small initial value [Eq. (5)], the physical values for Δ_0 and Δ_1 are in the same ballpark.

For the sake of generality, and acknowledging an approximate character of the scaling dimensions obtained from a one-loop RG, we shall leave β and β_v unspecified in the analytic expressions. An attempt to experimentally determine scaling exponents was made recently in Ref. [28], where a systematic change of the period of quantum oscillations with carrier density was interpreted in terms of Fermi velocity renormalization, giving a value $\beta_v = 0.5$–0.55, which is considerably larger than the one-loop RG result $\beta_v = (8/\pi^2 N) \approx 0.2$. This discrepancy is not yet understood. Yet, even a modest change in β_v may strongly impact the RG flow for the gap. Indeed, the enhancement factor $\Delta_0(\lambda_0)/\Delta_0^{(0)}$ is of order 50 for $\beta_v = 0.2$ and grows exponentially as β_v increases. Since the β_v value is probably underestimated by a one-loop RG, we pick a conservative value $\beta_v = 0.3$ for the plots in Fig. 1, giving $\beta = 2\beta_v = 0.6$ (with the superlattice period $\lambda_0 = 14$ nm). This suffices to illustrate the dramatic character of gap enhancement due to interactions.

We note that the large gap enhancement in Eq. (11) stems predominantly from the combinatorial factor of 3 in the exponent $3\beta - 2\beta_v$. This factor reflects the general structure of coupling to superlattice, which generates the bare DP gap at third order in the coupling m_3. We therefore expect that, while the exponent β value may change due to two-loop RG corrections, the exponent in Eq. (11) will remain large enough to generate substantial gap enhancement.

At length scales larger than λ_0, renormalization is suppressed by spatial oscillations in the m_3 term. In this regime, m_3 stops flowing and the gap Δ_1 stays constant, as shown by the horizontal line in Fig. 1 (stage 2). In contrast, because the effective Hamiltonian H_0' is $\mathbf{x}$ independent, modes with $|\mathbf{p}| < (2\pi/\lambda_0)$ continue to provide an enhancement to the gap at DP, giving

$$\Delta_0(\lambda > \lambda_0) = (\lambda/\lambda_0)^{\beta}\Delta_0(\lambda_0). \tag{12}$$

The RG flow of Δ_0 at stage 2 is described by the scaling exponent β which is smaller than the value $3\beta - 2\beta_v$ found for stage 1. Nevertheless, the growth of Δ_0 at stage 2 is still faster than that of velocity. As illustrated in Fig. 1, Δ_0 can grow by several orders of magnitude, reaching Δ_1 for large enough λ. For the parameters chosen in Fig. 1, Δ_0 (red line) overtakes Δ_1 (blue line), eventually making the gap at DP the largest gap in the system.

Renormalization of all the parameters in the system, including velocity v and the gap Δ_0, terminates either at an effective screening length set by the proximal gate or at a length scale generated self-consistently through a gap opening at DP. In the first case, the effective screening length is determined by the distance to the gate or by the screening length for the gate, whichever is larger. In the second case, realized for systems with remote gates or when the screening length is very large, RG terminates at a self-consistently defined length scale, λ_*, controlled by the gap opened at DP

$$\lambda_* = 2\pi/q_*, \qquad \hbar q_* = \Delta_0(\lambda_*)/v(\lambda_*), \tag{13}$$

where the λ dependence is obtained from RG flow. A similar approach was employed in Refs. [29,30] to estimate interaction-enhanced gaps opened at DP in chiral metallic carbon nanotubes. Under realistic conditions, as discussed above, we expect $\Delta_0 \ll \epsilon_0 = \frac{1}{2}\hbar v|\mathbf{b}|$. Hence, the self-consistent length scale satisfies $\lambda_* \gg \lambda_0$. In this case, plugging the dependence from Eqs. (9) and (12), we find $(\lambda_*/\lambda_0)^{1+\beta-\beta_v} = hv(\lambda_0)/[\lambda_0\Delta_0(\lambda_0)]$, giving

$$\Delta_0(\lambda_*) = \left(\frac{hv(\lambda_0)}{\lambda_0\Delta_0(\lambda_0)}\right)^{\beta/(1+\beta-\beta_v)}\Delta_0(\lambda_0) \propto \left(\frac{\lambda_0}{a}\right)^{\gamma}, \tag{14}$$

$\gamma = 3\beta - 2\beta_v - (\beta(1 + 3\beta - 3\beta_v)/1 + \beta - \beta_v)$. The predicted power-law dependence Δ_0 vs moiré wavelength λ_0 [Eq. (14)] can be used to directly probe the effects of interactions. Setting $\beta = 2\beta_v$ (see discussion above), the expression for the scaling exponent simplifies as

$$\gamma = 4\beta_v - \frac{2\beta_v(1 + 3\beta_v)}{1 + \beta_v} = \frac{\beta(2 - \beta)}{2 + \beta}. \tag{15}$$

For $\beta = (16/\pi^2 N) = 0.4$ (a lower bound for the exponent), we find $\gamma \approx 0.27$. This produces a characteristic angle-dependent gap [see Eq. (1)].

The predicted scaling [Eq. (1)] can be tested by comparing the gap values measured in G/h-BN systems with different twist angles, similar to the method used in Ref. [23] for replica Dirac peaks. Renormalization effects are maximized for structures with near-perfect crystal axis alignment, such as those in recent experiments [17,18,31]. Indeed, as illustrated in Fig. 1(a) Δ_0 can be enhanced by a factor of up to 10^3. A conservative estimate of the superlattice harmonic $m_3^{(0)} = \frac{1}{12}(53\ \text{meV})$ [10], would yield a gap as large as $\Delta_0 \approx 5$–40 meV [using Eq. (14) and $\beta = 2\beta_v = 0.4$–0.6]. This is close to recently observed gap values [16–18].

Besides the large gap values, interactions generate an anomalous hierarchy of gap sizes ($\Delta_0 > \Delta_1$) and a strong dependence of the gap Δ_0 on the twist angle [Eq. (1)]. These effects provide clear experimental signatures for the proposed scenario. The effective interaction strength can be tuned by adjusting the superlattice wavelength, which is done by rotating the G layer relative to the BN layer. This opens the doorway for realizing and exploring tunable interaction effects in graphene superlattices.

We thank D. Golhaber-Gordon, A. Geim, P. Jarillo-Herrero, J. Williams, and A. Young for useful discussions.

[1] D. Xiao, W. Yao, and Q. Niu, Phys. Rev. Lett. **99**, 236809 (2007).
[2] G. W. Semenoff, V. Semenoff, and F. Zhou, Phys. Rev. Lett. **101**, 087204 (2008).
[3] P. Avouris, Z. Chen, and V. Perebeinos, Nat. Nanotechnol. **2**, 605 (2007).
[4] R. D. Pisarski, Phys. Rev. D **29**, 2423 (1984).
[5] V. N. Kotov, B. Uchoa, V. M. Pereira, F. Guinea, and A. H. Castro Neto, Rev. Mod. Phys. **84**, 1067 (2012).
[6] J. R. Wallbank, A. A. Patel, M. Mucha-Kruczynski, A. K. Geim, and V. I. Fal'ko, Phys. Rev. B **87**, 245408 (2013).
[7] A. Mattausch and O. Pankratov, Phys. Rev. Lett. **99**, 076802 (2007).
[8] F. Varchon *et al.*, Phys. Rev. Lett. **99**, 126805 (2007).
[9] O. Pankratov, S. Hensel, and M. Bockstedte, Phys. Rev. B **82**, 121416(R) (2010).
[10] G. Giovannetti, P. A. Khomyakov, G. Brocks, P. J. Kelly, and J. van den Brink, Phys. Rev. B **76**, 073103 (2007).
[11] S. Y. Zhou, G.-H. Gweon, A. V. Fedorov, P. N. First, W. A. de Heer, D.-H. Lee, F. Guinea, A. H. Castro Neto, and A. Lanzara, Nat. Mater. **6**, 770 (2007).
[12] M. Kindermann, B. Uchoa, and D. L. Miller, Phys. Rev. B **86**, 115415 (2012).
[13] F. Guinea and T. Low, Phil. Trans. R. Soc. A **368**, 5391 (2010).
[14] C. H. Park, L. Yang, Y. W. Son, M. L. Cohen, and S. G. Louie, Nat. Phys. **4**, 213 (2008).
[15] C. H. Park, L. Yang, Y. W. Son, M. L. Cohen, and S. G. Louie, Phys. Rev. Lett. **101**, 126804 (2008).
[16] F. Amet, J. R. Williams, K. Watanabe, T. Taniguchi, and D. Goldhaber-Gordon, Phys. Rev. Lett. **110**, 216601 (2013).
[17] B. Hunt *et al.*, Science **340**, 1427 (2013).
[18] Cory Dean, APS Report No. M2.00003, 2013.
[19] V. N. Kotov, B. Uchoa, and A. H. Castro Neto, Phys. Rev. B **80**, 165424 (2009).
[20] C. R. Dean *et al.*, Nat. Nanotechnol. **5**, 722 (2010).
[21] L. A. Ponomarenko *et al.*, Nat. Phys. **7**, 958 (2011).
[22] B. Sachs, T. O. Wehling, M. I. Katsnelson, and A. I. Lichtenstein, Phys. Rev. B **84**, 195414 (2011).
[23] M. Yankowitz, J. Xue, D. Cormode, J. D. Sanchez-Yamagishi, K. Watanabe, T. Taniguchi, P. Jarillo-Herrero, P. Jacquod, and B. J. LeRoy, Nat. Phys. **8**, 382 (2012).
[24] In Eq. (5), we have assumed $\delta\phi = \phi_1 + \phi_2 + \phi_3 = 0$. For nonzero $\delta\phi$, we find the dependence $\Delta_0(\delta\phi) = \cos(\delta\phi)\Delta_0$.
[25] J. González, F. Guinea, and M. A. H. Vozmediano, Nucl. Phys. **B424**, 595 (1994); Phys. Rev. B **59**, R2474 (1999).
[26] O. Vafek, Phys. Rev. Lett. **98**, 216401 (2007).
[27] D. T. Son, Phys. Rev. B **75**, 235423 (2007).
[28] D. C. Elias *et al.*, Nat. Phys. **7**, 701 (2011).
[29] V. I. Talyanskii, D. S. Novikov, B. D. Simons, and L. S. Levitov, Phys. Rev. Lett. **87**, 276802 (2001).
[30] L. S. Levitov and A. M. Tsvelik, Phys. Rev. Lett. **90**, 016401 (2003).
[31] L. A. Ponomarenko *et al.*, Nature (London) **497**, 594 (2013).